Bovine hydroxyapatite-based scaffold accelerated the inflammatory phase and bone growth in rats with bone defect

by Chrismawan Ardianto

Submission date: 21-Feb-2023 04:39PM (UTC+0800)
Submission ID: 2019506925
File name: inflammatory_phase_and_bone_growth_in_rats_with_bone_defect.pdf (3M)
Word count: 7982
Character count: 41430

Original Research Article

JABFM Journal of Applied Biomaterials & Functional Materials

Journal of Applied Biomaterials & Functional Materials
1–12

DOI: 10.1177/22808000221149193
journals.sagepub.com/home/jbf
SAGE

Bovine hydroxyapatite-based scaffold accelerated the inflammatory phase and bone growth in rats with bone defect

Maria Apriliani Gani[1], Aniek Setiya Budiatin[2], Dewi Wara Shinta[2], Chrismawan Ardianto[2] and Junaidi Khotib[2]

Abstract

Hydroxyapatite (HA) is a biomaterial widely used to treat bone defect, such as due to traffic accident. The HA scaffold is obtained from synthetic HA or natural sources, such as bovine hydroxyapatite (BHA). This study aims to compare the characteristics and in vivo performance of BHA-based and HA-based scaffolds. For this purpose, the scaffold was formulated with gelatin (GEL) and characterised by SEM-EDX, FTIR and mini autograph. The defect model was carried out on the femur area of Wistar rats classified into three animal groups: defect, HA-GEL and BHA-GEL. Postoperatively (7, 14 and 28 days), the bone was radiologically evaluated, and stained with haematoxylin–eosin, anti-CD80 and anti-CD163. The BHA-GEL scaffold showed a regular surface and spherical particle shape, whereas the HA-GEL scaffold exhibited irregular surface. The BHA-GEL scaffold had higher pore size and compressive strength and lower calcium-to-phosphorus ratio than the HA-GEL scaffold. In vivo study showed that the expression of CD80 in the three experimental groups was not significantly different. However, the expression of CD163 differed significantly between the groups. The BHA-GEL group showed robust expression of CD163 on day 7, which rapidly decreased over time. It also showed increased osteoclasts, osteoblasts and osteocytes cell count that contributed to the integrity of the defect area. In conclusion, the BHA-based scaffold exhibited the desired physical and chemical characteristics that benefit in vivo performance versus the HA-based scaffold. Thus, the BHA-based scaffold may be used as a bone graft.

Keywords

Bone inflammation, carbonated hydroxyapatite, traffic accident, scaffold characteristics, bone remodelling, osteoconductive

Date received: 18 March 2022; revised: 17 October 2022; accepted: 18 December 2022

Introduction

Bone defect is a serious condition caused by pathological circumstances.[1,2] Bones can heal themselves through self-healing mechanisms. However, this mechanism is inconvenient for large gap sizes, leading to various complications. Bone grafting is a surgical procedure that accelerates bone growth in the defect area by using biomaterials.[1,3] It is known that the inflammatory response is one of the critical defence mechanisms involved in bone grafting.[3] It is reported that chronic inflammation caused delay the bone remodelling and lead to bone healing failure by increasing fracture healing time and the rate of complications.[4–6]

Macrophage polarisation is one event that modulates the inflammatory response. Polarised macrophages are calcified into classically activated macrophages (M1) and alternatively activated macrophages (M2).[7] To prevent

[1]Doctoral Program of Pharmaceutical Sciences, Faculty of Pharmacy, Universitas Airlangga, Surabaya, Indonesia
[2]Department of Pharmacy Practice, Universitas Airlangga, Surabaya, Indonesia

Corresponding author:
Junaidi Khotib, Department of Pharmacy Practice, Universitas Airlangga, Jl Mulyorejo Campus C, Gedung Nanizar Zaman Joenoes, Surabaya, East Java 60115, Indonesia.
Email: junaidi-k@ff.unair.ac.id

implantation failure, a bone scaffold should not induce a chronic inflammatory response. This can happen by the abundant presence of M2 cells in the early stages of inflammation.[7,8] It is reported that robust expression of M2 surface marker at the early stage controlled the inflammation at later time points.[9] In addition to the inflammation phase, bone remodelling also plays an important role in bone tissue reconstruction.[10] A scaffold should possess osteoconductivity properties, which induce bone growth at the defect area. This is mediated by the remodelling process, such as migration of bone cells to the defect site, which subsequently causes osteogenic differentiation and induces a series of molecular actions that accelerate bone growth in the defect area.[11,12]

Hydroxyapatite (HA) is a material widely used as a bone graft.[13] It is a calcium phosphate derivative with a chemical formula and properties similar to inorganic minerals found in bones and teeth.[14,15] Synthetic hydroxyapatite has been produced with a wide range of physicochemical properties. This difference in characteristics aims to provide the best therapeutic outcomes when HA is used as a bone graft.[16] However, autologous bone grafting is still the gold standard in clinical use. The application of autologous bone graft induced bone growth, did no harm to the patient and gave superior outcomes compared to synthetic graft.[17,18] However, because the material is obtained from the patient's body, the availability of bone for this graft is very limited, and morbidity is often found at the bone donor site.[17]

Bovine hydroxyapatite (BHA) is natural hydroxyapatite extracted from bovine bone.[6,19,20] BHA has similar characteristics to human bone, one of which BHA contains a carbonate substitution group similar to human HA, which is not found in synthetic HA.[19,21] It has been reported that HA-containing carbonate (carbonated HA) increases osteoblast proliferation, thereby accelerating the synthesis of new bone.[22,23]

Based on our preliminary study, BHA as a single material exhibited physical and chemical characteristics that may contribute to the osteoconductivity properties of BHA-based scaffolds.[19] Therefore, an in vivo comparative study of BHA-based and HA-based scaffolds was conducted. Calcium phosphates are known as brittle materials. Because of this, the mechanical stability of these materials and other characteristics should be a concern before implementation in vivo. In this study, BHA/HA was formulated with gelatin (GEL) as the bone scaffold.[3,24–26] The addition of GEL helps in increased the compressive strength of biomaterials, In general, the addition of polymers such as gelatine (GEL) helped increase the compressive strength and resulted in a controllable degradation rate of the scaffold.[27,28] The aim of this study was to investigate the in vivo performance of the BHA-based scaffold, specifically inflammatory response through M1 and M2, and osteoconductivity.

Material and methods

Scaffold fabrication

BHA powder was previously extracted from bovine as previous report.[19] Briefly, the bovine bones were cut and boiled in the opened chamber, followed by boiling in a pressurised tank. The bones were then soaked into 95% ethanol. After that, calcination was then conducted in 1000°C for 2 h to produce BHA powder. BHA and HA powder (cas number 1306-06-5) were used as the main materials of the scaffolds. The average hydrodynamic particle size of BHA and HA were 4074 ± 622 nm and 7366 ± 875, respectively. The particle shape of BHA was irregular, while HA was round.

Two scaffolds, namely BHA-GEL and HA-GEL, were fabricated. Briefly, distilled water was heated at 37°C using a water bath. GEL type B (Cartino, Samut Prakan, Thailand) (2 g) was added to heated distilled water (10 mL), and the mixture was stirred. Subsequently, BHA or HA (10 g) was added to 5 mL of previously prepared 20% GEL solution. The mixture was stirred and sieved using a mesh (size: 1.0 mm) and dried at 37°C. The granules (25 mg) were moulded into an implant (diameter: 2 mm) using a hydraulic press (2 ton; Graseby-Specac Ltd., Orpington, Kent, UK).

Scaffold characterisation

Pore size, morphology and calcium-to-phosphorus (Ca/P) ratio of the scaffold were examined using a scanning electron microscope connected with energy dispersive X-Ray spectroscopy (SEM-EDX, Inspect-S50; FEI, MA, USA). Pore size was determined based on SEM images with the help of ImageJ 1.52a software (National Institutes of Health, Bethesda, MD, USA), while Ca/P ratio was determined EDX results (three spectrum for each sample). The compressive strength of each scaffold ($n = 5$) was examined using a mini autograph (Original Equipment Manufacture; Autograph Microcomputer Control Universal Testing, LoadCell, YXC-1B, speed 5 mm/min). At the point of sample breakage, the compressive strength data were recorded automatically through software connected to a computer. The compressive strength was calculated as follows:

$$\text{Compressive strength } \left(\text{N}/\text{mm}^2\right) = \text{Force } \left(\text{Newton}\right) / \text{ Surface area } \left(\text{mm}^2\right) \quad (1)$$

The compressive strength of HA and BHA scaffolds was also determined to examine the effects of gelatine addition in each scaffold. Moreover, the chemical functional groups of each scaffold were examined using Fourier-transform infrared spectroscopy (FTIR, Bruker Alpha II; MA, USA).

Animals

The in vivo model was carried out using 36 male Wistar rats (Rattus norvegicus) (250–300 g) provided by the experimental animal centre of Faculty of Pharmacy, Universitas Airlangga. The rats were previously adapted to the laboratory environment and were housed under standard laboratory conditions on a 12 h light-dark cycle. All animal experiments were performed in accordance with the guidelines of the Animal Ethics Committee, Faculty of Veterinary Medicine, Universitas Airlangga, Surabaya, Indonesia. Rats were randomised into three groups ($n = 12$ per group). The first group did not receive a scaffold (defect group), the second group received the HA-GEL scaffold (HA-GEL group), and the third group received the BHA-GEL scaffold (BHA-GEL group). For in vivo use, scaffolds were sterilised by using ultraviolet light for several hours. All experimental animals were anaesthetised with a combination of ketamine (35 mg/kg, intraperitoneally) and xylazine (2.5 mg/kg, intraperitoneally). Subsequently, the area of the femur was shaved and an incision was performed. The distal area of the femur was drilled (diameter: 2.2 mm, depth: 2.0 mm) and the scaffold (HA-GEL or BHA-GEL) was implanted accordingly. The wound was sutured, disinfected with povidone-iodine, and covered with gauze. Ampicillin (25 mg/kg, intraperitoneally) was administered to prevent infection. Wound care was carried out for 7 days postoperatively or until wound healing. The rats were sacrificed on days 7, 14 and 28 by an overdose of propofol (600 mg/kg, intraperitoneally). The femur was removed and preserved through immersion in 10% formalin solution for ⩾3 days.

Haematoxylin–eosin staining

Haematoxylin–eosin (HE) staining was carried out to observe the bone cells (osteoclasts, osteoblasts and osteocytes) using standard procedures based on our previous studies.[3,29] The femur was decalcified with 10% ethylenediaminetetraacetic acid solution (pH 7.4, room temperature), which was changed every 3 days for 2 months. The decalcified bone samples were implanted in a paraffin block. Briefly, the paraffin blocks were prepared by dehydrating the tissue with ethanol (70%–100%, 60 min each). Next, cleansing was performed with xylol (thrice, 15 min each), and liquid paraffin infiltration was conducted with transfer performed thrice (60 min each, in an incubator at 60°C). The tissue was subsequently immersed in liquid paraffin and cooled at room temperature. Moreover, the tangential longitudinal section was made on paraffin blocks by using a rotary microtome (thickness: 4–6 µm).

HE staining was performed by dipping the histological slide in xylol thrice (5 min each), hydration with alcohol 70%–96% (2 min each), and rinsing under running water (10 min). The slide was soaked in Mayer's haematoxylin (15 min), rinsed under running water, and placed in 1% eosin solution (30 s). The slide was subsequently dehydrated through immersion in alcohol 80%–96% thrice (15 min, each) and mounted using an EZ mount.

Immunohistochemistry staining

Immunohistochemistry (IHC) staining was carried out to examine the expression of M1 and M2 surface markers. The procedure was conducted based on our previous studies.[3,29] Briefly, prior to IHC staining, the histological slide was deparaffinated using xylol (thrice, 5 min each), rehydrated using alcohol (70%–absolute, 4 min), and rinsed under running water (5 min). Subsequently, the slide was blocked using endogenous peroxide 0.5% (5 min) and rinsed with running water (5 min). Furthermore, antigen retrieval was carried out using a decloaking chamber; the slide was cooled for approximately 20 min, washed with phosphate-buffered saline (PBS; 3 min), and snipper blocked for 15 min. The slide was incubated with rabbit anti-rat CD80 (Bioss, Cat# bs-2211R, 1:250 dilution) or rabbit anti-rat CD163 (Bioss, Cat# bs-2527R, 1:250 dilution) for 60 min, and washed with PBS (3 min). Moreover, universal linking was carried out on the slide (20 min), followed by washing with PBS (3 min). Next, Trekavidin-horseradish peroxidase labelling was conducted on the slide (10 min), followed by washing with PBS (3 min). The slide was reacted with Chromogen DAB + Buffer Substrate (2–5 min) and washed with running water (5 min). The slide was counterstained with haematoxylin (1–2 min) and washed twice under running water (5 min each). Subsequently, the slide was dehydrated with alcohol (70%–absolute, 5 min), cleansed with xylol (thrice, 5 min each), mounted (EcoMount), and covered with a cover glass.

Histophotometric quantification

Histophotometric quantification was conducted by an investigator who was blinded to the group allocation by observing the histological slide under a microscope (CX22LED; Olympus, Tokyo, Japan) at a magnification of 400×. The number of osteoblasts, osteoclasts and osteocytes in the slide was counted based on the number of each cell in five different fields based on the morphology of each cell. Moreover, the expression of CD80 and CD163 was presented as immunoreactive score (IRS). Cell counts and IRS value were presented as mean ± standard error of the mean.

Radiology examination

The bone integrity was examined through X-ray radiography and analysed using the ImageJ 1.52a (National Institutes of Health, Bethesda, MD, USA) software. With an 8-bit colour depth, the colour threshold of the images

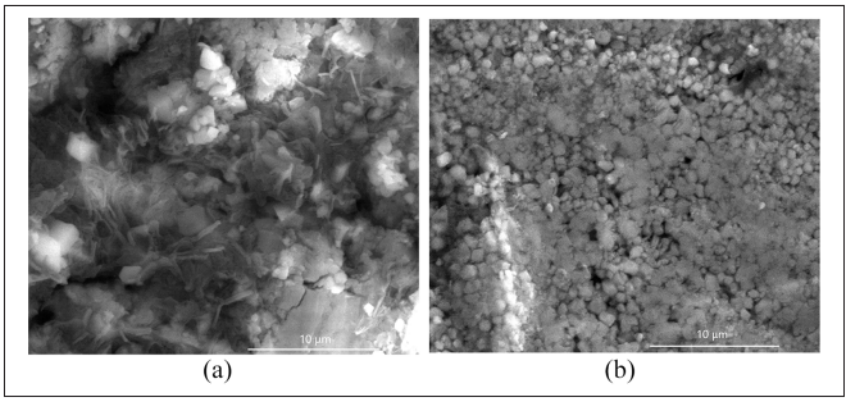

Figure 1. Surface morphology of the HA-GEL (a) and BHA-GEL (b) scaffolds observed using SEM with 10,000× magnification.

was set between 56 and 87 to clarify bone growth at the defect site.[30]

Statistical analysis

The Shapiro–Wilk test was used to determine the normality of data distribution. Meanwhile, a heterogeneity test was carried out using Levene's test to determine the data variance. Mann–Whitney analysis was used to assess the significance of the scaffold characteristic data. In vivo data were analysed using the Kruskal–Wallis test. All statistical tests were performed using the SPSS version 24.0 (IBM Corporation, Armonk, NY, USA) software.

Results

Scaffold characteristics

Physical and chemical characteristics are the factors that determine the osteoconductivity of a bone scaffold. We observed the following physical characteristics of the HA-GEL and BHA-GEL scaffolds: surface morphology, pore size and compressive strength. In terms of the surface morphology, the HA-GEL scaffold had an irregular surface, whereas the BHA-GEL scaffold had a more regular surface and each particle tended to be spherical (Figure 1). The BHA-GEL scaffold had higher pore size and compressive strength compared to the HA-GEL scaffold. The pore size of the HA-GEL and BHA-GEL scaffolds was $0.361 \pm 0.036\,\mu m$ and $0.633 \pm 0.089\,\mu m$, respectively (Mann–Whitney U test, $p = 0.035$; Figure 2(a)). The compressive strength of HA-GEL and BHA-GEL scaffolds was 40.766 ± 4.513 MPa and 61.714 ± 6.163 MPa, respectively (Mann–Whitney U test, $p = 0.041$; Figure 2(b)). Furthermore, this study also proved that the addition of GEL increases the compressive strength of the scaffolds. Scaffolds containing no GEL had lower compressive strength than those containing scaffolds (Mann–Whitney U test, $p < 0.041$; Figure 2(b)).

The present study also evaluated the chemical characteristics of BHA-GEL and HA-GEL scaffolds. It was shown that all materials had carbonate and phosphate groups present at a wavenumber of $1455\,cm^{-1}$ and $1000–1100\,cm^{-1}$, respectively (Figure 3). Moreover, the addition of GEL added the absorption region of wavelength $1575–1480\,cm^{-1}$, which corresponds to the amide II functional group (Figure 3). This study also examined the Ca/P ratio of BHA-GEL and HA-GEL scaffolds (Figure 4, Table 1). The Ca/P ratio was calculated based on the percentage of calcium and phosphorus obtained from three different spectra. According to the results, the BHA-GEL scaffold had a lower Ca/P ratio than the HA-GEL scaffold (Mann–Whitney U test, $p < 0.0001$; Table 1).

In vivo performance

To assess the in vivo performance, HA-GEL and BHA-GEL scaffolds were implanted into Wistar rats for 7, 14 and 28 days. Based on the present study, the experimental animals experienced weight loss immediately after the surgery. However, subsequently, the growth of the animals was normal based on their bodyweight (Figure 5). There was no significant difference in the bodyweight between the three animal groups at all time points.

Based on the results of histological staining with anti-CD80, the group of animals in which biomaterials were implanted exhibited high expression of CD80 on day 7; nevertheless, these levels were decreased on days 14 and 28 (Figure 6(a)). However, there was no significant difference in the IRS for CD80 at the three examined time points (Figure 6(b)). Notably, based on the results, the expression pattern of CD163 in the defect group was uncertain. Quantitative data also supported this finding; the IRS for CD163 in this group did not differ significantly between days 7, 14 and 28. On the other hand, the HA-GEL and BHA-GEL groups exhibited a more regular pattern of CD163 expression; the expression of this protein decreased

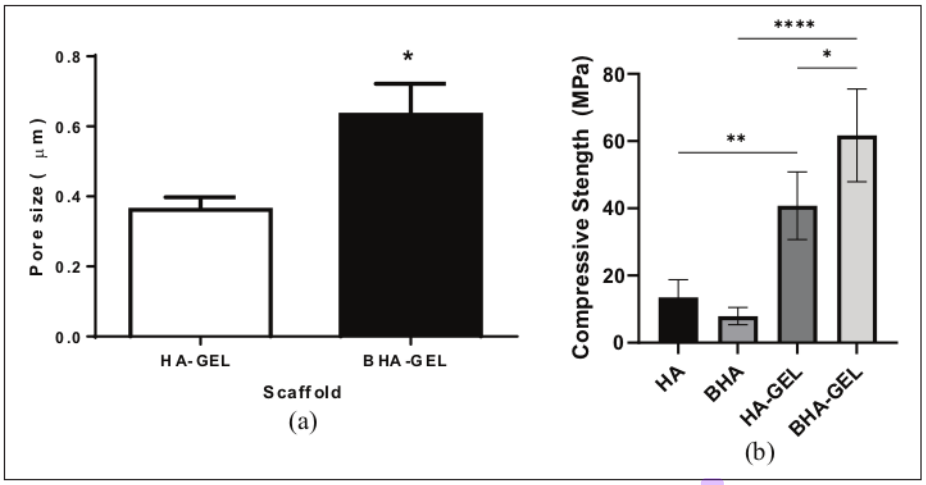

Figure 2. Pore size (a) and compressive strength (b) of the HA-GEL and BHA-GEL scaffolds. Each bar shows the mean ±SEM value. *$p < 0.05$ based on the Mann–Whitney *U* test.

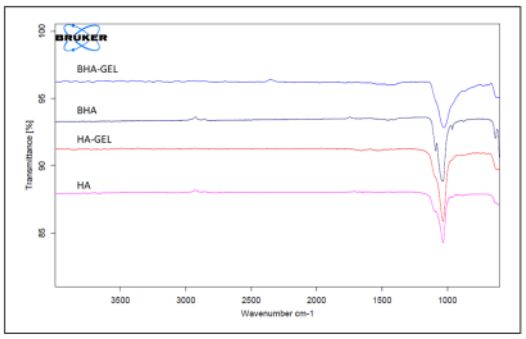

Figure 3. FTIR spectra of BHA-GEL, HA-GEL, BHA and HA. Arrows; amide II absorption region.

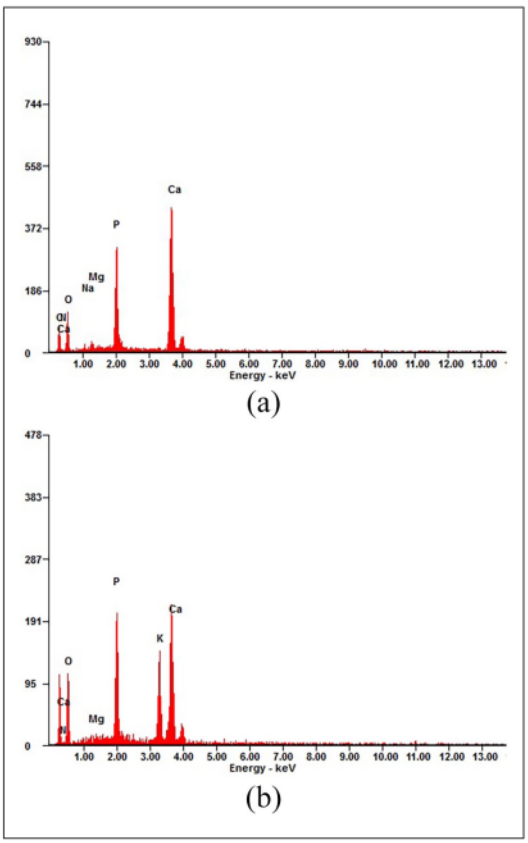

Figure 4. EDX spectrum of the HA-GEL (a) and BHA-GEL (b) scaffolds.

over time (Figure 7(a)), and the IRS for CD163 in these two groups differed significantly (Figure 7(b)). The IRS for CD163 in the HA-GEL group on days 7, 14 and 28 was 80.000 ± 4.082, 60.000 ± 17.321 and 15.000 ± 2.887, respectively. Meanwhile, the IRS for CD163 in the BHA-GEL group was 90.000 ± 0.000, 35.000 ± 16.583 and 22.500 ± 2.500, respectively. The IRS for CD163 on days 7 and 28 in the two scaffold groups exhibited similar statistical significance (Kruskal–Wallis test, $p < 0.05$; Figure 7(b)). However, on days 7 and 14, the IRS for CD163 in the HA-GEL group was not statistically significant (Kruskal–Wallis test, $p = 1.000$; Figure 7(b)). In contrast, in the BHA-GEL group, the IRS for CD163 at the same time point was statistically significant ($p = 0.047$; Figure 7(b)). These findings suggest that CD163 expression was decreased in the early implantation phase in the BHA-GEL group, but not in the HA-GEL group.

Table 1. Ca/P ratio of HA-GEL and BHA-GEL scaffold (mean ± SEM).

Scaffold		Calcium (Ca)		Phosphorus (P)		Ca/P ratio	Mean ± SEM of Ca/P ratio
		Weight (%)	Atomic (%)	Weight (%)	Atomic (%)		
HA-GEL	Spectrum 1	38.76	21.73	17.77	12.89	1.69	1.63 ± 0.03
	Spectrum 2	42.41	26.72	20.40	16.62	1.61	
	Spectrum 3	43.06	27.45	20.71	17.08	1.61	
BHA-GEL	Spectrum 1	28.54	17.22	15.94	12.44	1.38	1.44 ± 0.03*
	Spectrum 2	28.92	17.28	15.26	11.79	1.47	
	Spectrum 3	29.41	17.76	15.50	12.11	1.47	

*$P < 0.0001$ compared to HA-GEL based on Mann Whitney test.

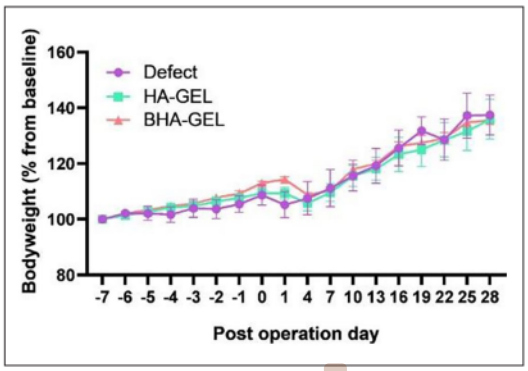

Figure 5. Rat bodyweight before and after surgery. There was no statistical difference in rat bodyweight between the three experimental groups based on the Kruskal–Wallis test. Each point shows the mean ± SEM.

Based on the results of HE staining, implantation of the BHA-GEL scaffold increase the number of osteoclasts, osteoblasts and osteocytes to the defect area (Figure 8(a)). This is supported by the histophotometric quantification of each type of cells (Figure 8(b)). On day 7, the number of osteoblasts in the BHA-GEL group was higher than that counted in the defect group. Notably, the number of osteoclasts and osteocytes in the BHA-GEL group was higher than those determined in the HA-GEL and defect groups (Figure 8(a)). hereas, in the HA-GEL group, robust count of these three cells was observed later on day 14.

Furthermore, the increased number of osteoblast and osteoclast in the BHA-GEL group accelerated the synthesis of new bone matrix. This was demonstrated by the robust presence of osteocytes noted on day 28 (Figure 8(b)) and the covered bone defect area in the BHA-GEL group compared with the other two groups (Figure 9).

Discussion

The characteristics of a bone tissue scaffold play an important in determining in vivo performance. The physical (e.g. surface morphology, particle shape and size and compressive strength) and chemical characteristics of the scaffold determine its interactions with cells present in the bone tissue microenvironment.[26,31–33] Based on our preliminary study, BHA had a hexagonal particle shape.[19] However, due to the addition of GEL, the morphology of the BHA-GEL scaffold particles in the present study was more spherical. On the other hand, the HA-GEL scaffold had an irregular surface, similar to the morphology of HA particles previously reported by Ahmad et al.[34] The surface morphology of the scaffold contributes to its interaction with inflammatory and osteogenic cells. Lebre et al. reported that HA with a spherical particle shape was associated with better immune response than those with other shapes.[31] This is because the spherical particle shape does not prolong the inflammatory response of the host.[31] Furthermore, the spherical particle shape supports the proliferation of osteoblasts and osteoclasts by increasing the expression of their osteogenic markers in vitro.[35,36]

Another critical factor in determining the interaction of bone cells with the biomaterial is the pore size of the scaffold. In the present study, the pore size values of BHA-GEL and HA-GEL scaffolds was similar to that in human, which was reported to be 0.1–0.77 µm.[37] SEM images by Yanagihara et al.[38] also showed that pore size of rat bone was less than 1 mm. Moreover, the BHA-GEL scaffold had a larger pore size than the HA-GEL scaffold. Scaffolds with large pore sizes induce macrophage infiltration, leading to secretion of pro-inflammatory cytokines by the cells and elimination of debris in the defective tissue.[33] These findings also suggested the acceleration of other involved processes, such as vascularisation and remodelling.[3]

In general, the pore size of the scaffold affects its compressive strength. Therefore, in the present study, the compressive strength of the HA-GEL and BHA-GEL scaffolds was evaluated. Based on the results, the BHA-GEL scaffold exhibited higher compressive strength than the HA-GEL scaffold. This demonstrated that the large pore size of the BHA-GEL scaffold did not reduce its strength. This may be attributed to the chemical bond present between BHA and GEL. GEL contains an $R\text{-}COO^-$; it is

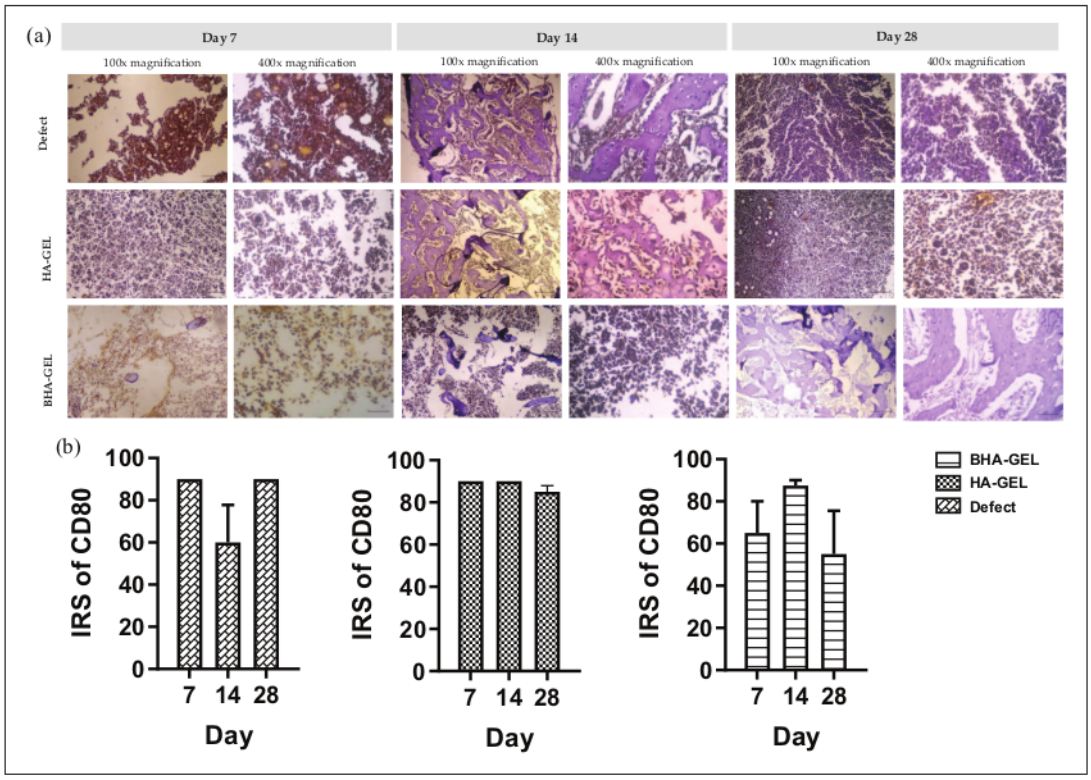

Figure 6. Representative histological images of the augmented region stained using CD80 immunohistochemical staining (a), and IRS value of CD80 (b) of the defect, HA-GEL, and BHA-GEL groups on days 7, 14 and 28. Each bar shows the mean ±SEM. Scale bar 100× magnification = 200 µm; 400× magnification = 50 µm.

suggested that this ion interacts with the $Ca^{2}+$ in HA. This complex subsequently interacts with the PO_4^{3-} and forms critical size nuclei, which are useful for HA crystal formation.[24,25] Moreover, the compressive strength of the BHA-GEL scaffold is the closest to that of the human cortical bone (100–230 MPa), and slightly higer than the human bone tensile strength reported by Fischer et al.[39] This compressive strength of BHA-GEL was also the closest to the rat femur bone, which was reported as 126.6 ± 19.7 and 167.3 ± 42.2 MPa for metaphyseal and diaphyseal specimens, respectively.[37]These hard characteristics of BHA-GEL scaffolds may prevent the premature degradation of the scaffold in vivo.[26]

Moreover, this study also examined the functional substitution groups in BHA-GEL and HA-GEL scaffolds, as well as BHA and HA scaffolds. The study showed that all material had the characteristics of calcium phosphate with carbonate and phosphate groups present at a specific wavenumber. The addition of GEL added the absorption region of wavelength 1575–1480 cm^{-1}, which corresponds to the amide II functional group.[40,41] This confirmed the presence of GEL. GEL helps in replacing the damaged extracellular matrix (ECM). Besides that, GEL contains the arginine–glycine–aspartic acid (RGD) sequence that is essential for stable relationships between the cells and the surrounding ECM, and helps in cell attachment and adhesion in the fabricated scaffolds.[42,43]

As one of the calcium phosphate materials, the CaP components of HA will further undergo dissolution to $Ca^{2}+$ and PO^{3-} when exposed to liquid.[44] In this study, the Ca/P ratio of the BHA-GEL scaffold was lower than that of the HA-GEL scaffold. This is consistent with the results of a study conducted by Szcześ et al.[14] which demonstrated that natural HA has a lower Ca/P ratio than synthetic HA. It has been postulated that materials with Ca/P of 1.67 are ideal for bone grafts. This is because Ca/P ratio of 1.67 is similar to HA Ca/P value in bone tissue.[32,45] Moreover, a study by Liu et al. showed that Ca/P of 1.67 induced osteoclast-mediated osseointegration in vivo. However, the is no enough justification for this Ca/P ratio to osteoblasts activity. Furthermore, studies started to report that other Ca/P with a wide variety of Ca/P ratios can also induce osteoblasts proliferation and differentiation, contributing to better in vivo performance.[46–48] It was reported there are

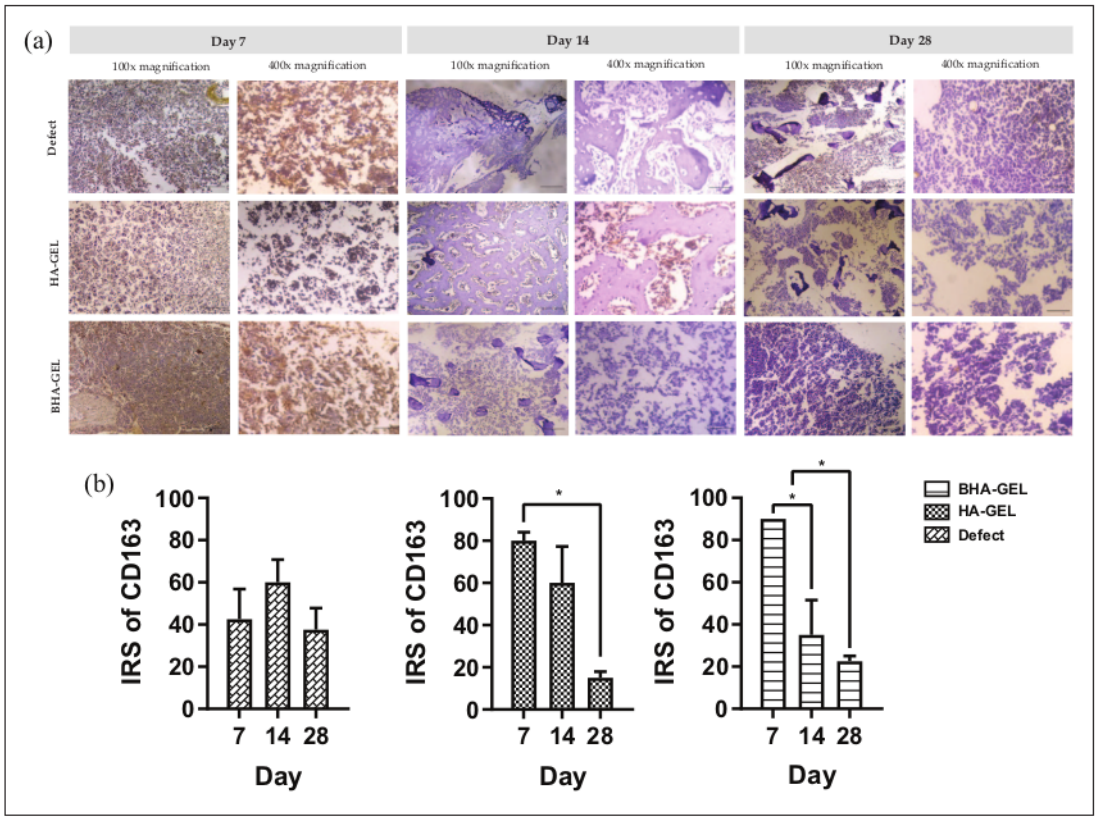

Figure 7. Representative histological images of the augmented region stained using CD163 immunohistochemical staining (a), and IRS value of CD163 (b) of the defect, HA-GEL, and BHA-GEL groups on days 7, 14 and 28. Each bar shows the mean ± SEM. *$p < 0.05$ based on the Kruskal–Wallis test. Scale bar 100× magnification = 200 µm; 400× magnification = 50 µm.

no differences in alkaline phosphatase activity and collagen production for calcium phosphate with Ca/P ratios ranging from 0.5 to 2.5.[46] It also reported that differences in Ca/P ratio did not affect the cell viability and percentage of vascular area in vivo.[47] A study by Choy et al. showed that a β-TCP with Ca/P ratio of 2.0 was reported to produce higher bone tissue area compared to other β-TCP with a Ca/P value of 1.62.[48] Because of this, the Ca/P ratio is not the only parameter in determining the osteogenic properties of bone grafts. Other factors such as the physical properties also should be considered. The BHA-GEL and HA-GEL scaffolds in this study also had similar Ca/P values with rat bone, which were reported to range from 1.74 to 2.14.[49]

The effect of scaffold implantation on the inflammatory response in vivo was examined in Wistar rats by staining for M1 and M2 surface markers, namely CD80 and CD163. CD80 is a membrane protein found in antigen-presenting cells, including M1.[50] CD80 expression was positively correlated with the release of pro-inflammatory cytokines, such as interleukin 6 (IL6).[51] On the other hand, CD163 is a protein that belongs to the cysteine-rich receptor scavenger family (SRCR). This protein is expressed on the membrane of macrophages and monocytes, particularly M2c macrophages, which possess anti-inflammatory activity.[52,53] CD80 and CD163 have been used as markers for M1 and M2, respectively, particularly in studies of biomaterials.[8] Based on the present findings, the number of M1 did not significantly decrease over time in the experimental groups. We indicate this because the surface marker used is also expressed by other inflammatory cells.[50] Unlike M1, the HA-GEL and BHA- GEL scaffolds showed high M2 counts in the early implantation phase which decreased over time. However, the lowest M2 count was found in the BHA-GEL group. Badylak et al.[54] reported that the expression of CD163 as a marker of M2 was also dominant in the use of autologous tissue grafts after 1 week in vivo. The use of autologous tissue graft is the current gold standard for bone tissue reconstruction. The robust count of M2 at the early stage reduced the inflammatory response of the host. A subsequent significant reduction in M2 at later points supported this finding.[9]

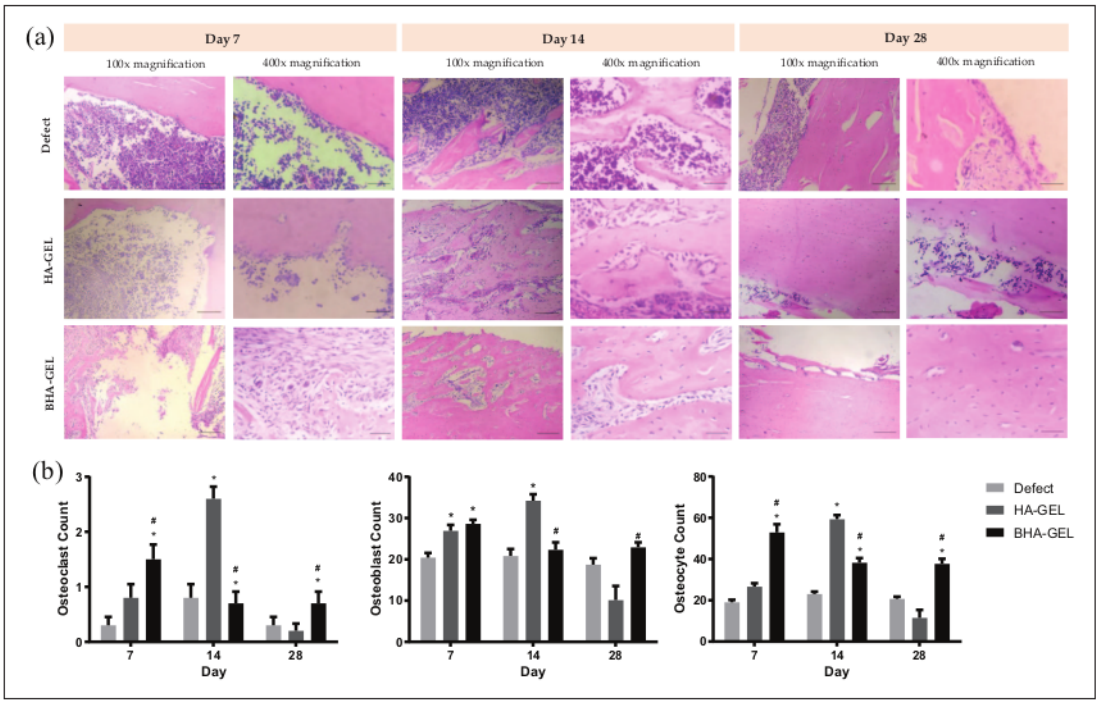

Figure 8. Representative histological images of the augmented region stained using haematoxylin–eosin staining (a), and osteoclasts, osteoblasts, osteocytes cell counts (b) from the defect, HA-GEL and BHA-GEL groups on days 7, 14 and 28. Each bar shows the mean ± SEM. $^{*}p < 0.05$ compared with defect, $^{\#}p < 0.05$ compared with HA-GEL based on the Kruskal–Wallis test. Scale bar 100× magnification = 200 µm; 400× magnification = 50 µm.

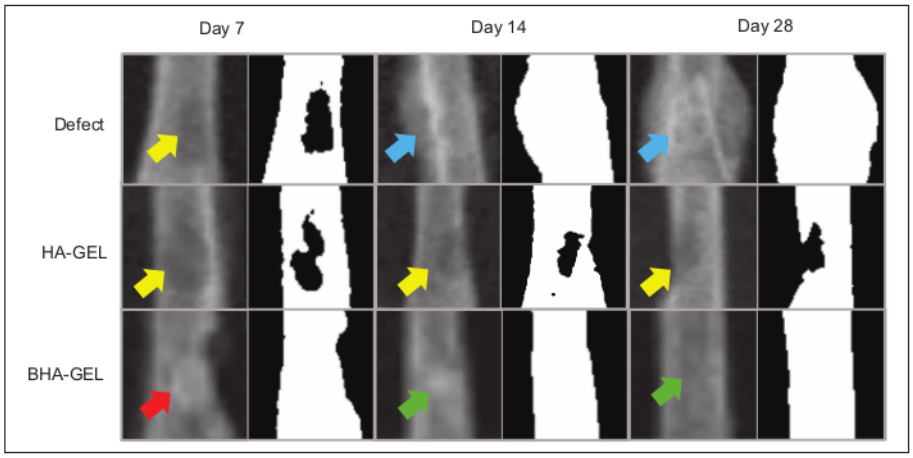

Figure 9. Representative radiological images of the augmented region of the defect, HA-GEL, and BHA-GEL groups on days 7, 14 and 28. Left, X-Ray images; right, thresholded version of X-Ray images. Yellow arrow, defect; blue arrow, swollen bone; red arrow, scaffold; green arrow, new bone. HA-GEL scaffold was degraded at day 7, while the BHA-GEL scaffold was not and still present in day 7.

Based on radiological data, unlike the HA-GEL scaffold, there was no premature degradation of the BHA-GEL scaffold. Instead, animals in the BHA-GEL group experienced early bone growth in the defect area compared with the HA-GEL and defect groups. In addition, an increased count of bone cells was observed in rats that

received the BHA-GEL scaffold. Material for bone and dental application should be non-toxic to the surrounding cells.[55] Increased count of osteoclasts, osteoblasts and osteocytes in the defect site indicated that the scaffold was not toxic. Moreover, osteoblasts play a role in the synthesis of new bone. Ha et al.[56] showed that HA accelerated osteoblast differentiation via changes in the expression of osteogenic genes (e.g. alkaline phosphatase and osteopontin) which are mediated by the extracellular signal-regulated kinase 1/2 (ERK1/2) signalling. pathway. Furthermore, our review also showed that other signalling pathways (e.g. p38, Wnt and bone morphogenetic protein 2) were involved in osteoblast differentiation mediated by HA.[57] The activation of a particular signalling pathway may depend on the different physical and chemical characteristics of HA.[57] Thus, designing HA with specific characteristics is important, which can exert the desired molecular effects.

The accelerated bone repair associated with the BHA-GEL scaffold is also affected by its chemical composition. Similar to human bones, BHA is characterised by a carbonate group substitution that distinguishes it from synthetic HA.[19] Naturally, the carbonate group accounts for 2%–8% of the total weight of human bone HA.[58–60] In our preliminary study, the carbonate substitution was observed in Fourier transform infrared spectra with a wavenumber of 1455 cm^{-1}.[19] However, this was not observed in spectra for synthetic HA.21 HA-containing carbonate is also referred to as carbonated HA. Several studies found that carbonated HA induced a higher proliferation rate of pre-osteoblasts than uncarbonated HA.[22] Carbonated HA also increased the collagen matrix gene expression compared with non-carbonated HA; this effect was also observed in osteoclasts.[61]

Carbonated HA was linked to higher cell viability and metabolism of pre-osteoclasts compared with non-carbonated HA.[22] Furthermore, BHA (also a carbonated HA) was associated with a higher percentage of new bone in a rabbit bone defect model 12 weeks after implantation.[23] Moreover, BHA also resulted in a higher percentage of bone-to-material contact than synthetic HA.[62] Bone-to-material contact is the percentage of direct contact of implants with materials at the microscopic level, which is a parameter for osseointegration.[35,62] Thus, it is suggested that the osteoconductivity of BHA was due to the substitution of the carbonate groups present on its apatite.

The present study had several limitations, one of which is that the M1 marker used was not specifically expressed on M1. Application of the double-staining IHC technique is necessary to overcome this limitation. However, the reported data are sufficient to describe the in vivo inflammatory response associated with the implantation of BHA-GEL and HA-GEL scaffolds, as well as their osteoconductivity.

Conclusions

Based on the present study, the BHA-based scaffold had a regular surface morphology and spherical particle shape, unlike the HA-based scaffold. The BHA-based scaffold also had a larger pore size, greater compressive strength, and lower Ca/P ratio compared with the HA-based scaffold. These characteristics beneficially contributed to the in vivo performance of the scaffold. The BHA-based scaffold accelerated the inflammatory phase by a high number of M2 at the early phase of implantation, which rapidly decreased over time. The BHA-based scaffold also accelerated the remodelling phase by increasing osteoclasts, osteoblasts and osteocytes cell count at the implanted site. This contributed to bone integrity in the defect area. Thus, the BHA-based scaffold can be potentially used as an orthopaedic implant. However, further in vitro study is warranted to elucidate the molecular mechanism of BHA and identify the signalling pathway involved in this process.

Acknowledgements

The authors thank the Faculty of Pharmacy, Universitas Airlangga for all support during the research.

Contributorship

Conceptualisation, M.A.G. and J.K.; methodology, M.A.G., J.K., and A.S.B.; software, M.A.G. and C.A.; validation, J.K. and C.A.; formal analysis, M.A.G.; investigation, M.A.G.; resources, J.K. and A.S.B.; data curation, D.W.S.; writing – original draft preparation, M.A.G.; writing – review and editing, M.A.G., and J.K.; visualisation, M.A.G.; supervision, J.K. and C.A.; project administration, D.W.S.; funding acquisition, J.K. All authors reviewed and edited the manuscript and approved the final version of the manuscript

Declaration of conflicting interests

The author(s) declared no potential conflicts of interest with respect to the research, authorship, and/or publication of this article.

Funding

The author(s) disclosed receipt of the following financial support for the research, authorship, and/or publication of this article: This research was funded by the Ministry of Education and Culture of Republic of Indonesia, through PMDSU research scheme [grant number: 1207/UN3.14/PT/2020].

Guarantor

J.K.

ORCID iDs

Dewi Wara Shinta https://orcid.org/0000-0002-5175-5054
Junaidi Khotib https://orcid.org/0000-0002-8468-8441

References

1. Gani MA, Nurhan AD, Budiatin AS, Siswodihardjo S and Khotib J. Predicting the molecular mechanism of glucosamine in accelerating bone defect repair by stimulating osteogenic proteins. *J Basic Clin Physiol Pharmacol* 2021; 32: 373–377.
2. Stewart S, Bryant SJ, Ahn J, et al. Bone regeneration. In: *Clinical aspects of regenerative medicine*. Amsterdam, Netherlands: Elsivier Inc, 2015, pp.313–333.
3. Budiatin AS, Gani MA, Samirah S, et al. Bovine hydroxyapatite-based bone scaffold with gentamicin accelerates vascularization and remodeling of bone defect. *Int J Biomater* 2021; 2021: 1–7.
4. Khotib J, Utami NW, Gani MA and Ardianto C. The change of proinflammatory cytokine tumor necrosis factor α level in the use of meloxicam in rat model of osteoarthritis. *J Basic Clin Physiol Pharmacol* 2019; 30: 1–8.
5. Claes L, Recknagel S and Ignatius A. Fracture healing under healthy and inflammatory conditions. *Nat Rev Rheumatol* 2012; 8: 133–143.
6. Budiatin AS, Gani MA, Putri BRKH, et al. In vivo study of bovine hydroxyapatite - gelatin - hydroxypropyl methylcellulose with alendronate as injectable bone substitute composite in osteoporotic animal model. *J Adv Pharm Technol Res* 2022; 13: 261–265.
7. Li K, Shen Q, Xie Y, You M, Huang L and Zheng X. Incorporation of cerium oxide into hydroxyapatite coating regulates osteogenic activity of mesenchymal stem cell and macrophage polarization. *J Biomater Appl* 2017; 31: 1062–1076.
8. Linares J, Fernández AB, Feito MJ, et al. Effects of nanocrystalline hydroxyapatites on macrophage polarization. *J Mater Chem B* 2016; 4: 1951–1959.
9. Tang Y, Tong X, Conrad B and Yang F. Injectable and in situ crosslinkable gelatin microribbon hydrogels for stem cell delivery and bone regeneration in vivo. *Theranostics* 2020; 10: 6035–6047.
10. Sadowska JM and Ginebra MP. Inflammation and biomaterials: role of the immune response in bone regeneration by inorganic scaffolds. *J Mater Chem B* 2020; 8: 9404–9427.
11. Albrektsson T and Johansson C. Osteoinduction, osteoconduction and osseointegration. *Eur Spine J* 2001; 10(Suppl 2): S96–S101.
12. Lee SK, Han CM, Park W, Kim IH, Joung YK and Han DK. Synergistically enhanced osteoconductivity and anti-inflammation of PLGA/β-TCP/Mg(OH)2 composite for orthopedic applications. *Mater Sci Eng C* 2019; 94: 65–75.
13. Carvalho MS, Poundarik AA, Cabral JMS, da Silva CL and Vashishth D. Biomimetic matrices for rapidly forming mineralized bone tissue based on stem cell-mediated osteogenesis. *Sci Rep* 2018; 8(1): 14388.
14. Szcześ A, Hołysz L and Chibowski E. Synthesis of hydroxyapatite for biomedical applications. *Adv Colloid Interface Sci* 2017; 249: 321–330.
15. Oryan A, Hassanajili S, Sahvieh S and Azarpira N. Effectiveness of mesenchymal stem cell-seeded onto the 3D polylactic acid/polycaprolactone/hydroxyapatite scaffold on the radius bone defect in rat. *Life Sci* 2020; 257: 118038.
16. Ghiasi B, Sefidbakht Y, Mozaffari-Jovin S, et al. Hydroxyapatite as a biomaterial - a gift that keeps on giving. *Drug Dev Ind Pharm* 2020; 46: 1035–1062.
17. García-Gareta E, Coathup MJ and Blunn GW. Osteoinduction of bone grafting materials for bone repair and regeneration. *Bone* 2015; 81: 112–121.
18. Ong JC, Kennedy MT, Mitra A and Harty JA. Fixation of tibial plateau fractures with synthetic bone graft versus natural bone graft: A comparison study. *Ir J Med Sci* 2012; 181: 247–252.
19. Budiatin AS, Gani MA, Nilamsari WP, Ardianto C and Khotib J. The characterization of bovine bone-derived hydroxyapatite isolated using novel non-hazardous method. *J Biomim Biomater Biomed Eng* 2020; 45: 49–56.
20. Budiatin AS, Gani MA, Ardianto C, et al. The impact of glutaraldehyde on the characteristics of bovine hydroxyapatite-gelatin based bone scaffold as gentamicin delivery system. *J Basic Clin Physiol Pharmacol* 2021; 32: 687–691.
21. Bouropoulos N, Stampolakis A and Mouzakis DE. Dynamic mechanical properties of calcium alginate-hydroxyapatite nanocomposite hydrogels. *Sci Adv Mater* 2010; 2: 239–242.
22. Germaini M-M, Detsch R, Grünewald A, et al. Osteoblast and osteoclast responses to A/B type carbonate-substituted hydroxyapatite ceramics for bone regeneration. *Biomed Mater* 2017; 12: 035008.
23. Xu A, Zhou C, Qi W and He F. Comparison study of three hydroxyapatite-based bone substitutes in a calvarial defect model in rabbits. *Int J Oral Maxillofac Implants* 2019; 34: 434–442.
24. Chang MC, Ko CC and Douglas WH. Preparation of hydroxyapatite-gelatin nanocomposite. *Biomaterials* 2003; 24: 2853–2862.
25. Hu H, Huang B-W, Lee Y-T, et al. Dramatic improvement of the mechanical strength of silane-modified hydroxyapatite-gelatin composites via processing with cosolvent. *ACS Omega* 2018; 3: 3592–3598.
26. Prasadh S and Wong RCW. Unraveling the mechanical strength of biomaterials used as a bone scaffold in oral and maxillofacial defects. *Oral Sci Int* 2018; 15: 48–55.
27. El Fadhlallah PM, Yuliati A, Soesilawati P, et al. Biodegradation and compressive strength test of scaffold with different ratio as bone tissue engineering biomaterial. *J Int Dent Med Res* 2018; 11: 587–590.
28. Park HJ, Lee OJ, Lee MC, et al. Fabrication of 3D porous silk scaffolds by particulate (salt/sucrose) leaching for bone tissue reconstruction. *Int J Biol Macromol* 2015; 78: 215–223.
29. Setiawatie EM, Gani MA, Rahayu RP, et al. Nigella sativa toothpaste promotes anti-inflammatory and anti-destructive effects in a rat model of periodontitis. *Arch Oral Biol* 2022; 137: 105396.
30. Barbeck M, Kühnel L, Witte F, et al. Degradation, bone regeneration and tissue response of an innovative volume stable magnesium-supported GBR/GTR barrier membrane. *Int J Mol Sci* 2020; 21: eng1010927911422
31. Lebre F, Sridharan R, Sawkins MJ, Kelly DJ, O'Brien FJ and Lavelle EC. The shape and size of hydroxyapatite particles dictate inflammatory responses following implantation. *Sci Rep* 2017; 7(1): 2922.
32. Loh QL and Choong C. Three-dimensional scaffolds for tissue engineering applications: role of porosity and pore size. *Tissue Eng Part B Rev* 2013; 19: 485–502.

33. Abbasi N, Ivanovski S, Gulati K, Love RM and Hamlet S. Role of offset and gradient architectures of 3-D melt electrowritten scaffold on differentiation and mineralization of osteoblasts. *Biomater Res* 2020; 24(1): 16.
34. Ahmad M, Wahit MU, Abdul Kadir MR and Mohd Dahlan KZ. Mechanical, rheological, and bioactivity properties of ultra high-molecular-weight polyethylene bioactive composites containing polyethylene glycol and hydroxyapatite. *Sci World J* 2012; 2012: 1–13
35. Bernhardt A, Dittrich R, Lode A, Despang F and Gelinsky M. Nanocrystalline spherical hydroxyapatite granules for bone repair: in vitro evaluation with osteoblast-like cells and osteoclasts. *J Mater Sci Mater Med* 2013; 24: 1755–1766.
36. Zhang Y, Li Q, Li X, et al. Preparation and evaluation of two apatites with spherical nanocrystal morphology. *J Nanosci Nanotechnol* 2016; 16: 2384–2389.
37. Ogoshi K, Moriyama T and Nanzai Y. Decrease in the mechanical strength of bones of rats administered cadmium. *Arch Toxicol* 1989; 63: 320–324.
38. Yanagihara GR, Paiva AG, Gasparini GA, et al. High-impact exercise in rats prior to and during suspension can prevent bone loss. *Braz J Med Biol Res* 2016; 49(3): 49035086.
39. Fischer B, Kurz S, Höch A and Schleifenbaum S. The influence of different sample preparation on mechanical properties of human iliotibial tract. *Sci Rep* 2020; 10(1): 14836.
40. Pradini D, Juwono H, Madurani KA and Kurniawan F. A preliminary study of identification halal gelatin using quartz crystal microbalance (QCM) sensor. *Malaysian J Fundam Appl Sci* 2018; 14: 325–330.
41. Derkach SR, Kuchina YA, Baryshnikov AV, Kolotova DS and Voron'ko NG. Tailoring cod gelatin structure and physical properties with acid and alkaline extraction. *Polymers* 2019; 11: 1–17.
42. Yadav N and Srivastava P. Osteoblast studied on gelatin based biomaterials in rabbit bone bioengineering. *Mater Sci Eng C* 2019; 104: 109892.
43. Kim AY, Kim Y, Lee SH, Yoon Y, Kim WH and Kweon OK. Effect of gelatin on osteogenic cell sheet formation using canine adipose-derived mesenchymal stem cells. *Cell Transplant* 2017; 26: 115–123.
44. Shih YR, Hwang Y, Phadke A, et al. Calcium phosphate-bearing matrices induce osteogenic differentiation of stem cells through adenosine signaling. *Proc Natl Acad Sci U S A* 2014; 111: 990–995.
45. Dorozhkin SV. Calcium orthophosphates as bioceramics: State of the art. *J Funct Biomater* 2010; 1: 22–107.
46. Liu H, Yazici H, Ergun C, Webster TJ and Bermek H. An in vitro evaluation of the Ca/P ratio for the cytocompatibility of nano-to-micron particulate calcium phosphates for bone regeneration. *Acta Biomater* 2008; 4: 1472–1479.
47. Kohli N, Sharma V, Orera A, et al. Pro-angiogenic and osteogenic composite scaffolds of fibrin, alginate and calcium phosphate for bone tissue engineering. *J Tissue Eng* 2021; 12: 20417314211005610.
48. Choy CS, Lee WF, Lin PY, et al. Surface modified β-tricalcium phosphate enhanced stem cell osteogenic differentiation in vitro and bone regeneration in vivo. *Sci Rep* 2021; 11: 9234.
49. Tzaphlidou M, Speller R, Royle G and Griffiths J. Preliminary estimates of the calcium/phosphorus ratio at different cortical bone sites using synchrotron microCT. *Phys Med Biol* 2006; 51: 1849–1855.
50. Chen L and Flies DB. Molecular mechanisms of T cell co-stimulation and co-inhibition. *Nat Rev Immunol* 2013; 13: 227–242.
51. Jiménez-Uribe AP, Valencia-Martínez H, Carballo-Uicab G, et al. CD80 expression correlates with IL-6 production in THP-1-like macrophages costimulated with LPS and dialyzable leukocyte extract (Transferon®). *J Immunol Res* 2019; 2019: 2198508.
52. Møller HJ. Soluble CD163. *Scand J Clin Lab Invest* 2012; 72: 1–13.
53. Etzerodt A and Moestrup SK. CD163 and inflammation: biological, diagnostic, and therapeutic aspects. *Antioxid Redox Signal* 2013; 18: 2352–2363.
54. Badylak SF, Valentin JE, Ravindra AK, McCabe GP and Stewart-Akers AM. Macrophage phenotype as a determinant of biologic scaffold remodeling. *Tissue Eng Part A* 2008; 14: 1835–1842.
55. Setiawatie EM, Sari DS, Wahyudadi BS, et al. Viability of Nigella sativa toothpaste with SLS compared non-SLS on fibroblast cell culture. *J Int Dent Med Res* 2021; 12: 525–528.
56. Ha SW, Park J, Habib MM and Beck GR Jr. Nano-hydroxyapatite stimulation of gene expression requires fgf receptor, phosphate transporter, and Erk1/2 signaling. *ACS Appl Mater Interfaces* 2017; 9: 39185–39196.
57. Khotib J, Gani MA, Budiatin AS, Lestari MLAD, Rahadiansyah E and Ardianto C. Signaling pathway and transcriptional regulation in osteoblasts during bone healing: direct involvement of hydroxyapatite as a biomaterial. *Pharmaceuticals* 2021; 14: 615.
58. Boskey AL and Coleman R. Aging and bone. *J Dent Res* 2010; 89: 1333–1348.
59. Jokanović V, Čolović B, Marković D, et al. Extraordinary biological properties of a new calcium hydroxyapatite/poly(lactide-co-glycolide)-based scaffold confirmed by in vivo investigation. *Biomed Tech* 2017; 62: 295–306.
60. Madupalli H, Pavan B and Tecklenburg MMJ. Carbonate substitution in the mineral component of bone: discriminating the structural changes, simultaneously imposed by carbonate in A and B sites of apatite. *J Solid State Chem* 2017; 255: 27–35.
61. Rupani A, Hidalgo-Bastida LA, Rutten F, Dent A, Turner I and Cartmell S. Osteoblast activity on carbonated hydroxyapatite. *J Biomed Mater Res - Part A 2012*; 100A: 1089–1096.
62. Lambert F, Bacevic M, Layrolle P, Schüpbach P, Drion P and Rompen E. Impact of biomaterial microtopography on bone regeneration: comparison of three hydroxyapatites. *Clin Oral Implants Res* 2017; 28: 201–207.

Bovine hydroxyapatite-based scaffold accelerated the inflammatory phase and bone growth in rats with bone defect

ORIGINALITY REPORT

9%	6%	6%	0%
SIMILARITY INDEX	INTERNET SOURCES	PUBLICATIONS	STUDENT PAPERS

PRIMARY SOURCES

1	www.nature.com Internet Source	1%
2	www.researchsquare.com Internet Source	1%
3	www.karger.com Internet Source	1%
4	s-space.snu.ac.kr Internet Source	<1%
5	pure.manchester.ac.uk Internet Source	<1%
6	www.science.gov Internet Source	<1%
7	www.hindawi.com Internet Source	<1%
8	Yazhou Long, Katrin Bundkirchen, Pascal Gräff, Christian Krettek, Sandra Noack, Claudia Neunaber. "Cytological Effects of Serum Isolated from Polytraumatized Patients	<1%

	on Human Bone Marrow-Derived Mesenchymal Stem Cells", Stem Cells International, 2021 Publication	
9	dokumen.pub Internet Source	<1 %
10	journals.viamedica.pl Internet Source	<1 %
11	pubmed.ncbi.nlm.nih.gov Internet Source	<1 %
12	A Hadjipanteli, N Kourkoumelis, P Fromme, A Olivo, J Huang, R Speller. "A new technique for the assessment of the 3D spatial distribution of the calcium/phosphorus ratio in bone apatite", Physiological Measurement, 2013 Publication	<1 %
13	repositorio-aberto.up.pt Internet Source	<1 %
14	Xuezhong He, Xiaoming Yang, Esmaiel Jabbari. "Combined Effect of Osteopontin and BMP-2 Derived Peptides Grafted to an Adhesive Hydrogel on Osteogenic and Vasculogenic Differentiation of Marrow Stromal Cells", Langmuir, 2012 Publication	<1 %
15	www.quintessence-publishing.com Internet Source	<1 %

16	bioone.org Internet Source	<1 %
17	core.ac.uk Internet Source	<1 %
18	biomarkerres.biomedcentral.com Internet Source	<1 %
19	biosignaling.biomedcentral.com Internet Source	<1 %
20	Altaib Mohammed, Reda Saleh, Doaa Taiema, Abdel-Nasser Abdel-Hady, Asmaa, Metwally. "In Vivo Biocompatibility of β Tri-calicum Phosphate Versus White Portland Cement in Mandibular Bone Surgical Defect in Dogs", Egyptian Dental Journal, 2019 Publication	<1 %
21	Iain R. Gibson, William Bonfield. "Novel synthesis and characterization of an AB-type carbonate-substituted hydroxyapatite", Journal of Biomedical Materials Research, 2002 Publication	<1 %
22	Kaixuan Yu, Huimin Huangfu, Qiuyue Qin, Yi Zhang, Xinming Gu, Xinchan Liu, Yidi Zhang, Yanmin Zhou. "Application of Bone Marrow-Derived Macrophages Combined with Bone Mesenchymal Stem Cells in Dual-Channel Three-Dimensional Bioprinting Scaffolds for	<1 %

Early Immune Regulation and Osteogenic Induction in Rat Calvarial Defects", ACS Applied Materials & Interfaces, 2022
Publication

---

23 Liu, H.. "An in vitro evaluation of the Ca/P ratio for the cytocompatibility of nano-to-micron particulate calcium phosphates for bone regeneration", Acta Biomaterialia, 200809
Publication

<1 %

---

24 Teliang Lu, Siwen Yan, Haishan Shi, Jiandong Ye. "Synthesis, Characterization, In Vitro Cytological Responses, and In Vivo Bone Regeneration Effects of Low-Crystalline Nanocarbonated Hydroxyapatite", ACS Biomaterials Science & Engineering, 2023
Publication

<1 %

---

25 Xiangfeng Li, Tao Song, Xuening Chen, Menglu Wang, Xiao Yang, Yumei Xiao, Xingdong Zhang. "Osteoinductivity of Porous Biphasic Calcium Phosphate Ceramic Spheres with Nanocrystalline and Their Efficacy in Guiding Bone Regeneration", ACS Applied Materials & Interfaces, 2019
Publication

<1 %

---

26 www.biorxiv.org
Internet Source

<1 %

27	Ahmet Engin Pazarçeviren, Ayşen Tezcaner, Dilek Keskin, Serap Topsoy Kolukısa, Sedat Sürdem, Zafer Evis. "Boron-doped Biphasic Hydroxyapatite/β-Tricalcium Phosphate for Bone Tissue Engineering", Biological Trace Element Research, 2020 Publication	<1 %
28	Berna Kankilic, Eda Ciftci Dede, Petek Korkusuz, Muharrem Timuçin, Feza Korkusuz. "Chapter 3 Apatites for Orthopedic Applications", Springer Science and Business Media LLC, 2017 Publication	<1 %
29	Hyun Jung Park, Kyung Dan Min, Min Chae Lee, Soo Hyeon Kim et al. "Fabrication of 3D porous SF/β-TCP hybrid scaffolds for bone tissue reconstruction", Journal of Biomedical Materials Research Part A, 2016 Publication	<1 %
30	Rukmani Sridharan, Katelyn J. Genoud, Daniel J. Kelly, Fergal J. O'Brien. "Hydroxyapatite Particle Shape and Size Influence MSC Osteogenesis by Directing the Macrophage Phenotype in Collagen-Hydroxyapatite Scaffolds", ACS Applied Bio Materials, 2020 Publication	<1 %
31	Sandra Van Watering, Sylvia P G Mannesse-Lazeroms, Joop H Dijkman, Pieter S Hiemstra.	<1 %

"Effect of neutrophil serine proteinases and defensins on lung epithelial cells: modulation of cytotoxicity and IL-8 production", Journal of Leukocyte Biology, 1997
Publication

32	St-Pierre, J.-P.. "Three-dimensional growth of differentiating MC3T3-E1 pre-osteoblasts on porous titanium scaffolds", Biomaterials, 200512 Publication	<1 %
33	Susmita Bose, Dongxu Ke, Himanshu Sahasrabudhe, Amit Bandyopadhyay. "Additive manufacturing of biomaterials", Progress in Materials Science, 2018 Publication	<1 %
34	Zongliang Wang, Li Chen, Yu Wang, Xuesi Chen, Peibiao Zhang. "Improved Cell Adhesion and Osteogenesis of op-HA/PLGA Composite by Poly(dopamine)-Assisted Immobilization of Collagen Mimetic Peptide and Osteogenic Growth Peptide", ACS Applied Materials & Interfaces, 2016 Publication	<1 %
35	discovery.researcher.life Internet Source	<1 %
36	ijms.sums.ac.ir Internet Source	<1 %

37	journals.biologists.com Internet Source	<1 %
38	mro.massey.ac.nz Internet Source	<1 %
39	ndl.ethernet.edu.et Internet Source	<1 %
40	scholarworks.umass.edu Internet Source	<1 %
41	www.wjgnet.com Internet Source	<1 %
42	"Marine-Derived Biomaterials for Tissue Engineering Applications", Springer Science and Business Media LLC, 2019 Publication	<1 %
43	Kortekaas, K. A., J. H. Lindeman, M. I. Versteegh, E. van Beelen, R. Kleemann, and R. J. Klautz. "Heart failure determines the myocardial inflammatory response to injury", European Journal of Heart Failure, 2013. Publication	<1 %
44	Qiaomu Tian, Huinan Liu. "Electrophoretic deposition and characterization of nanocomposites and nanoparticles on magnesium substrates", Nanotechnology, 2015 Publication	<1 %

Exclude quotes	Off	Exclude matches	Off
Exclude bibliography	On		

Bovine hydroxyapatite-based scaffold accelerated the inflammatory phase and bone growth in rats with bone defect

GRADEMARK REPORT

FINAL GRADE

/0

GENERAL COMMENTS

Instructor

PAGE 1

PAGE 2

PAGE 3

PAGE 4

PAGE 5

PAGE 6

PAGE 7

PAGE 8

PAGE 9

PAGE 10

PAGE 11

PAGE 12